Biodiversity and Conservation Science

Great Victoria Desert Vegetation Monitoring Report 2020-21

Ricky van Dongen[1], Jaume Ruscalleda Alvarez[2], Kathryn Sinclair[2], Katherine Zdunic[1] and Paul Rampant[1]

[1] Department of Biodiversity, Conservation and Attractions

[2] Great Victoria Desert Biodiversity Trust

Great Victoria Desert Vegetation Mapping

August 2021

Department of Biodiversity, Conservation and Attractions

GOVERNMENT OF WESTERN AUSTRALIA

Department of Biodiversity, Conservation and Attractions
Locked Bag 104
Bentley Delivery Centre WA 6983
Phone: (08) 9219 9000
Fax: (08) 9334 0498

www.dbca.wa.gov.au

This report/document/publication was prepared by Ricky van Dongen

Questions regarding the use of this material should be directed to:
Remote Sensing Research Officer
Biodiversity and conservation Science
Department of Biodiversity, Conservation and Attractions
Locked Bag 104
Bentley Delivery Centre WA 6983
Phone: 9219 9571
Email: Ricky.vandongen@dbca.wa.gov.au

The recommended reference for this publication is:
van Dongen R., Ruscalleda Alvarez J., Sinclair K., Zdunic K. and Rampant P. 2021: *Great Victoria Desert Vegetation Monitoring Report*, Department of Biodiversity, Conservation and Attractions, Perth.

This document is available in alternative formats on request.

Contents

1 Introduction v
1.1 Landsat satellite imagery v
2 Methodology vi
2.1 Satellite Data..vi
2.2 Classification of Lidar data 7
2.3 Vegetation cover and fire recovery.. 8
3 Results and Discussion... 9
References.. 21

Figures

Figure 1: Management area and Landsat scene location within the Great Victoria Desert IBRA bioregion. vi
Figure 2: Training point numbers per tile.. 7
Figure 3:Distributions of LiDAR-derived NSM values and means of the Red-Green-Blue high resolution imagery for the three cover classes. In the NSM plots, y-axis units are in meters; in the Red-Green-Blue mean plots, y-axis units are digital numbers (DN). 10
Figure 4: The percentage composition of the three classes of the 30 tiles............... 11
Figure 5: Cover type from the calibration tiles against a range of indices from Landsat data. The “max” plots use the maximum index value from 2019, whereas the “dif” plots use the difference between the maximum and minimum index values from 2019. 12
Figure 6: Regression of vegetation cover (classified using LiDAR and RGB variables) against a range of indices from Landsat imagery.................................... 14
Figure 7: Vegetation cover map from a Landsat image, captured on 23/11/2020, of the management area in the Great Victoria Desert.................................. 15
Figure 8: A years since last burn map of the management area in the Great Victoria Desert. Fire maps from 1995 to 2020 were used to create the map. 16
Figure 9: A predicted fire recovery dataset across the management area within the Great Victoria Desert.. 18
Figure 10: A time series graph of vegetation cover at check point 1........................ 19
Figure 11: A time series graph of vegetation cover at check point 2........................ 19
Figure 12: A time series graph of vegetation cover at check point 3........................ 20

Summary

This report presents satellite imagery-based vegetation monitoring options for the Great Victoria Desert (GVD).

LiDAR and high resolution RGB imagery is used to assess if Landsat imagery can separate, and therefore monitor, three different types of cover (bare ground, grasses and trees/shrubs). The highest correlations were when LiDAR and RGB imagery was used to derive combined grass and tree/shrub cover against the i35 (Lehmann et al. 2013) index (r^2 = 0.918;) and SATVI (Marsett et al. 2006) index (r^2 = 0.923). However, these correlations only drop slightly with vegetation cover classifications using only the RGB imagery (0.904 for i35 and 0.916 for SATVI). This result demonstrates that high resolution RGB imagery is sufficient to provide classified reference tiles for satellite imagery. It was also found that Landsat-derived spectral indices do not significantly relate with grass cover, whereas tree/shrub and tree/shrub combined with ground covers show moderate and strong relationships.

Landsat imagery was also used to generate models of vegetation cover percentage (combined grass and tree/shrub) and fire recovery percentage. The key driver of vegetation cover change in the GVD is fire. Therefore, a simple “years since last burn” (YSLB) dataset is a good predictor of vegetation cover. However, following fire, the time taken for vegetation cover to return to pre-burn levels is also dependent on rainfall. In this environment rainfall can be sporadic and variable across the landscape. Two methods are recommended here to track this recovery and help determine when an area might be suitable to burn, or where the area of greatest fire risk is located.

The first method is to produce a fire recovery dataset. This is created using the YSLB and annual vegetation cover datasets. It shows the percent to which vegetation cover has recovered since the previous fire. As such, areas with values above 100 are above a vegetation cover value where they are known to have burnt and areas with values below 100 are below a vegetation cover value where they are known to have burnt. Areas with values greater than 100 are therefore likely to have a greater fire risk. It is hoped that this dataset will better characterize the ability of an area to carry fire than that provided by fire history maps (both *years since last burn* maps and *rainfall since last burn* maps).

The second method is to produce graphs which track the changes in vegetation cover at a point. These can be produced for points of interest to provide greater detail of burn/recovery patterns.

Further studies should investigate if higher resolution satellite imagery (such as Sentinel-2 10 m pixel data) could be related with grass or tree/shrub cover (separately) better than Landsat. Additionally, it would be interesting to know if the approach to map fire recovery can be extrapolated to other parts of the Western Desert by using the same model, or by creating a new model based on aerial imagery already available for a wider part of it.

1 Introduction

The contemporary fire pattern in the Great Victoria Desert (GVD) is characterised by cycles of large areas burnt by hot fires in spring and summer (Haydon et al., 2000). Traditional Owners in this region have an interest in managing Country, and fire management is an integral component of their management. Currently unmanaged fire is having adverse impacts on economic, environmental, social and cultural values (Burrows, Gill, and Sharples 2018). It is therefore one of the critical threats facing the Great Victoria Desert. Contemporary bushfires follow good rainfall periods, typically after summer storms. Whilst fire has always been part of the desert ecosystem, the scale and intensity of fire in the Great Victoria Desert has increased at a dramatic rate.

Contemporary fuel management programs are informed from fire scar maps and prescribed fire plans. In the central deserts of Australia, localised fire history is mapped from field observations. However, across larger scales, imagery captured from satellites is used to interpret fire history and delineate fire scar boundaries, and to predict and manage wildfire risk in the future.

Fire history in the form of “years since last burn” maps is commonly used as reliable predictors of when an area might be suitable to burn again. In this form the yslb map is, in many ways, a proxy for vegetation cover. Vegetation (fuel) cover is a key component when determining the likelihood of fire spread, the rate of spread and flame height (Burrows, Gill, and Sharples 2018). However, greater detail, in terms of the type of vegetation and burn potential would greatly benefit fire management and biodiversity conservation planning.

1.1 Landsat satellite imagery

Landsat satellite imagery is being used in the project to provide a detailed fire history and to map and monitor changes to vegetation cover. The imagery has become a key dataset for monitoring and modelling environmental change (Wulder et al. 2012). The Landsat series of satellites captures imagery at 30 m resolution across several spectral bands, of which six were used for this study (red, green, blue, near infrared, short-wave infrared 1 and short-wave infrared 2). The satellites began capturing data in 1972 with the Landsat 1 satellite (at 60 m pixel resolution) with regular captures from 1987 (at 30 m pixel resolution). The archive of Landsat imagery is available for download, free of charge, from the United States Geological Survey

Landsat satellite data is used extensively to map the progress of active fires (Schroeder et al. 2016), compile detailed fire histories (Ruscalleda-Alvarez, Moro, and Van Dongen submitted) and evaluating post-fire recoveries (Qarallah et al. 2021).

2 Methodology

2.1 Satellite Data

The location of the management area and Landsat scene used in the study are shown in Figure 1.

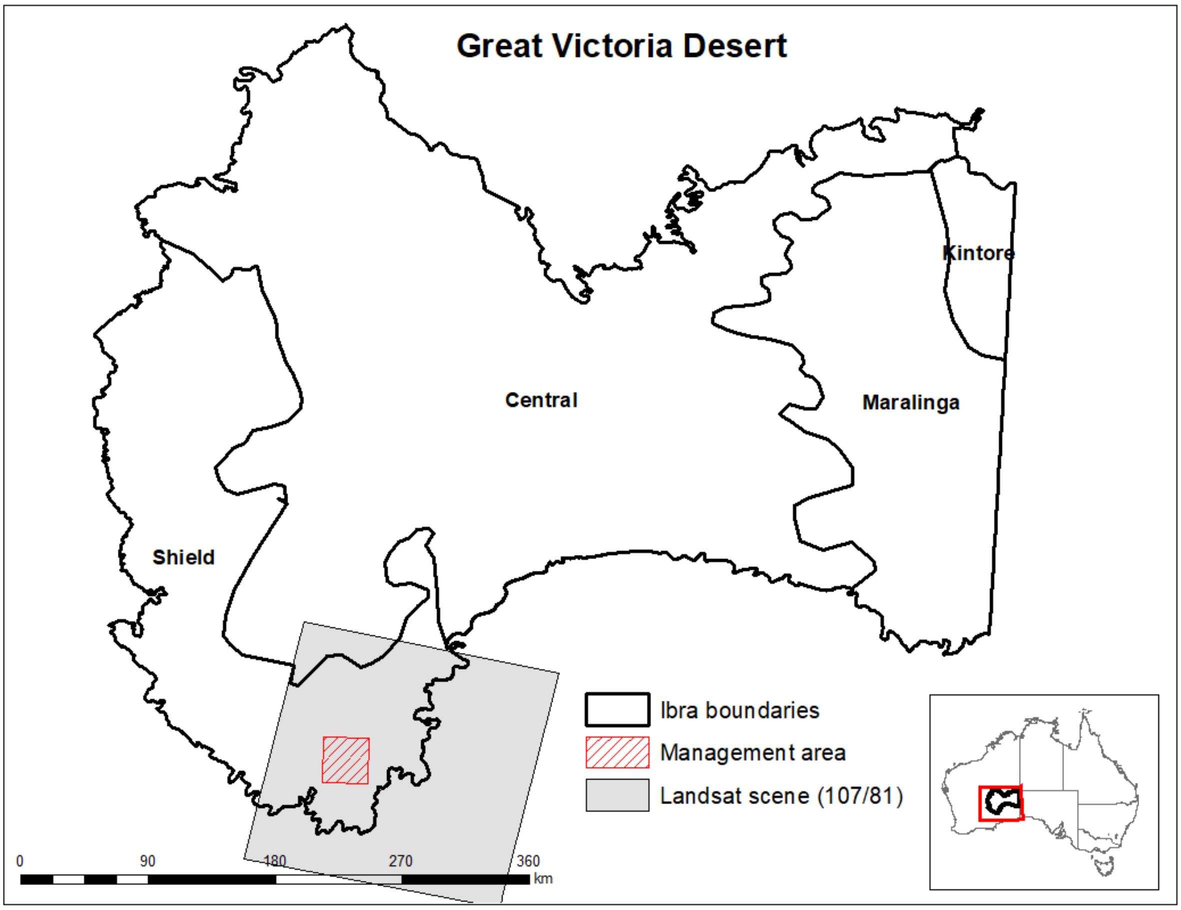

Figure 1: Management area and Landsat scene location within the Great Victoria Desert IBRA bioregion.

2.2 Classification of Lidar data

Light detection and ranging (LiDAR) data was captured for the GVDBT across a number of narrow strips within the GVD. The data was captured for the purposes of identifying malleefowl mounds. LiDAR data was processed by the data provider (Anditi) and delivered as a point cloud dataset, at 4 points per m^2. In parallel, RGB (red, green and blue bands) imagery at 6cm resolution was also collected. The point cloud data was converted to a normalised surface model (NSM) at 1 m resolution using LASTools.

To test the ability of Landsat satellite data to separate ground, grasses and trees/shrubs, the LiDAR data and the high resolution RGB imagery were clipped into 30 test tiles. Each tile was 90 by 90 m and consisted of 6 cm resolution RGB imagery and a 1 m resolution normalised surface model (NSM). The location of each tile was manually selected to cover the range of vegetation types visible in the RGB imagery, for example, from areas of largely bare ground, to areas with a mix of grasses and shrubs, and areas of dense tree/shrub cover.

Within each tile, around 30 training points were added, with a maximum of 10-11 in each cover types (ground, grasses and trees/shrubs) (Figure 2).

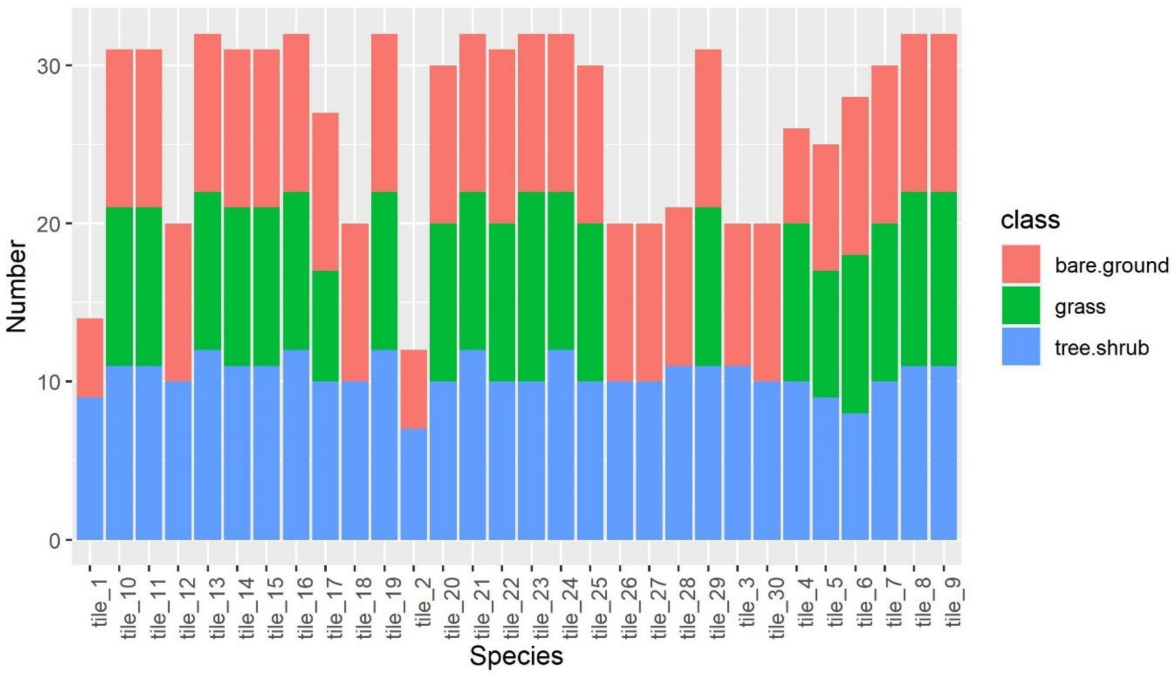

Figure 2: Training point numbers per tile.

Each tile was segmented using eCognition Developer (v10.0). The segmentation process groups areas with similar pixel values into small polygons called segments. The segmentation scale was set to 20, and the shape and area parameters were set to 0.5. The segments for each tile were exported as separate shapefiles, with each polygon/segment attributed with the mean value from the red, green and blue bands, along with the mean and maximum NSM values.

In R (R Core Team, 2014), the training points for each tile were intersected with the corresponding segments. This resulted in the training points now being attributed with the identified class and variables from the segmentation. This data was used in the ranger random forest package (Wright & Ziegler, 2017) as training data to produce a separate model for each tile. The 30 individual models were then applied to the respective tiles to produce a series of classified tiles. The proportions of ground, grasses and tree/shrub per tile were then regressed against a range of indices from Landsat satellite data (Table 1). This training tile classification process was repeated using only variables from the RGB data.

Table 1: Landsat imagery indices (band numbers relate to Landsat satellites 5 to 7).

Index	Formula
i35	$(\rho band3 + \rho band5)/2$
STVI	$\frac{\rho band5 \times \rho band3}{\rho band4}$
NBR	$\frac{\rho band4 - \rho band7}{\rho band4 + \rho band7}$
NDMI	$\frac{\rho band5 - \rho band7}{\rho band5 + \rho band7}$
NDVI	$\frac{\rho band4 - \rho band3}{\rho band4 + \rho band3}$
SATVI	$\frac{\rho band5 - \rho band3}{\rho band5 + \rho band3 + 0.5}(1.5) - \frac{\rho band7}{2}$
SWRI	$(\rho band3 \,/\, \rho band5)$

2.3 Vegetation cover and fire recovery

Vegetation cover datasets from within the management area were created using Landsat satellite data for each year from 1988 to 2020, where cloud free imagery was available. The time of year for each image selected was centred on November.

From the process described in the previous section a formula to convert i35 index values to vegetation cover was derived (Equation 1). This equation was applied to the selected Landsat data (1988 to 2020) to create a vegetation cover image for each year.

The modelled annual vegetation cover datasets were combined with the YSLB dataset to produce a fire recovery dataset. Using an iterative process in R, for each year in the YSLB datasets the vegetation cover values prior to the burn were calculated, these were then subtracted from the maximum post fire vegetation cover values. In the resulting image areas with a negative value have a current vegetation cover level lower than the last time they burnt and areas with a positive value have cover levels higher than the last time they burnt.

3 Results and Discussion

The degree to which variables from the LiDAR data differ between the ground, grass and tree\shrub cover class can be visually assessed in the boxplots shown in Figure 3. The classes show a reasonable degree of separability in the mean of the red, green and blue bands. However, grass and ground overlap in variables from the NSM. This indicates that the four points per square meter LiDAR data was ineffective at distinguishing the height of grasses such as *triodia* from the surrounding ground level. This indicates that the bands in the RGB data are more important when separating grass from bare ground. The large difference between the quartile ranges of grass and trees/shrubs suggests that the LiDAR data (Max_NSM and Mean_NSM) is influential in separating these classes.

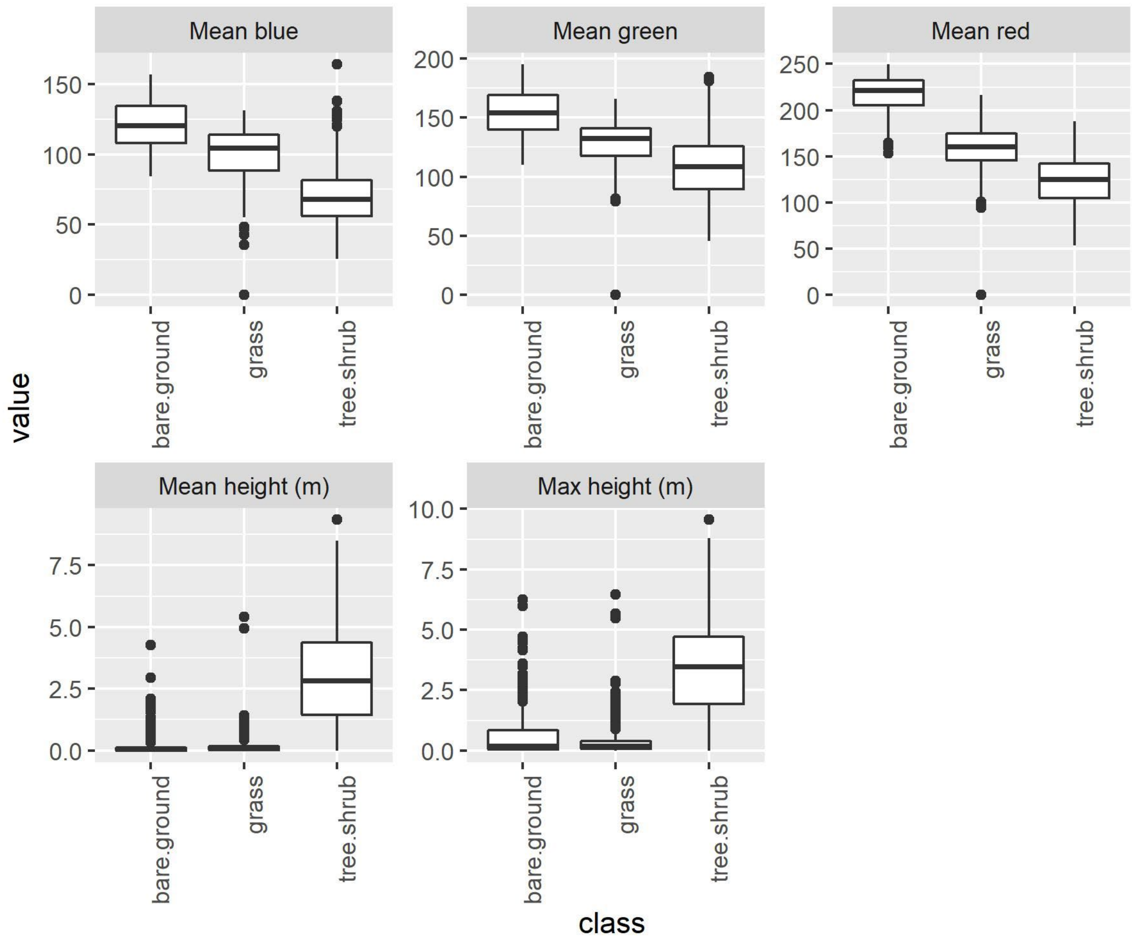

Figure 3:Distributions of LiDAR-derived NSM values and means of the Red-Green-Blue high resolution imagery for the three cover classes. In the NSM plots, y-axis units are in meters; in the Red-Green-Blue mean plots, y-axis units are digital numbers (DN).

Across the 30 tiles, the mean accuracy of the classification using LiDAR point cloud-derived data and high resolution RGB imagery data was 98.2 %, with a minimum of 93.3 %. When variables from the LiDAR point cloud-derived data (NSM) is removed the mean accuracy drops to 92.6 % with a minimum of 64.8 %.

Table 2: Classification accuracy of the tiles with and without LiDAR data (NSM).

	Classification with LiDAR and RGB imagery	Classification with RGB imagery
Mean	98.2 %	92.6 %
Minimum	93.3 %	64.8 %
Maximum	100 %	100 %

The percent of each cover class across the 30 tiles as a result of the classification process (using RGB and NSM data) is shown in Figure 4.

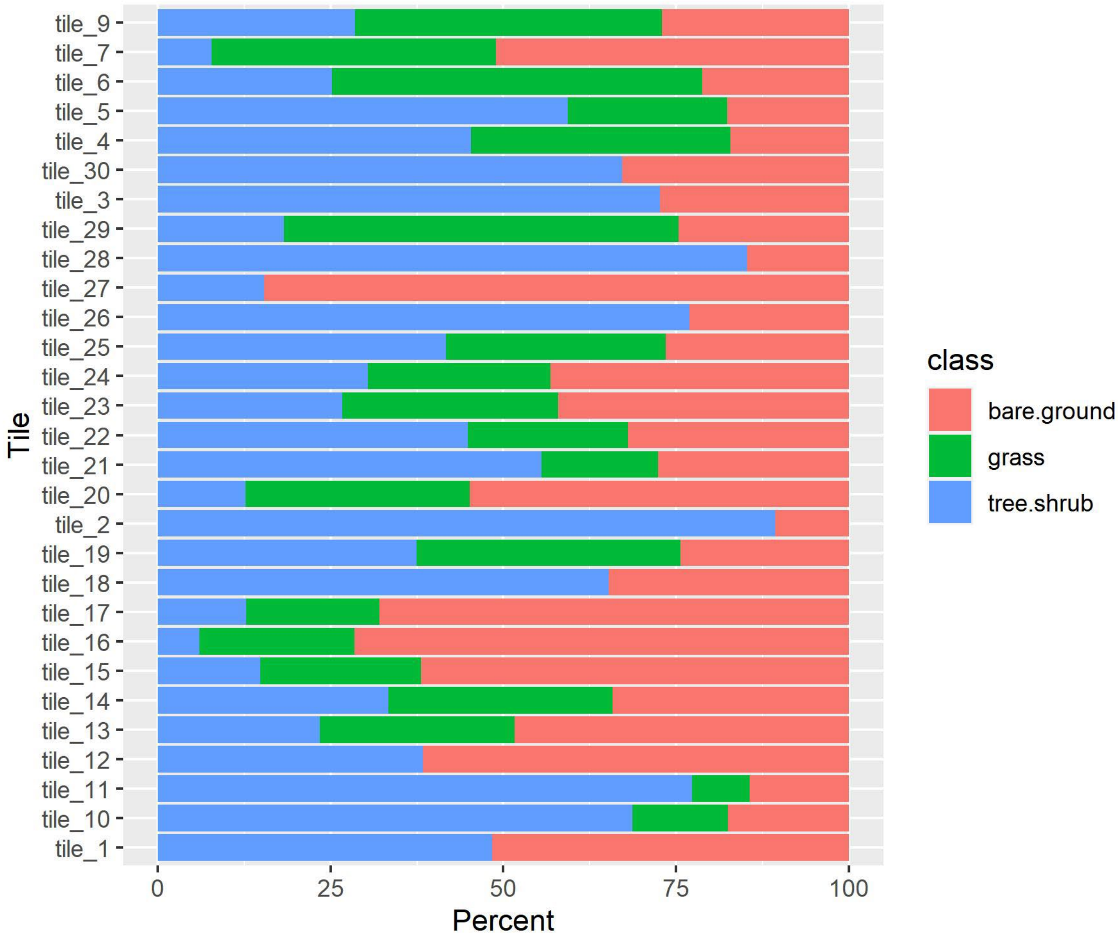

Figure 4: The percentage composition of the three classes of the 30 tiles.

Graphs showing the ordinary least squares regression between a range of spectral indices from Landsat imagery against the class composition of each tile is shown in Figure 5. The graphs show that percent grass has no relationship against indices tested. Trees and shrubs recorded a moderate relationship with the maximum value from both i35 and NDVI. The strongest correlation appears to be when LiDAR and RGB data are used in the classification of bare ground against the maximum i35 (Table 2). This is only marginally higher then when the classification of bare ground is carried out with only variables from the RGB imagery.

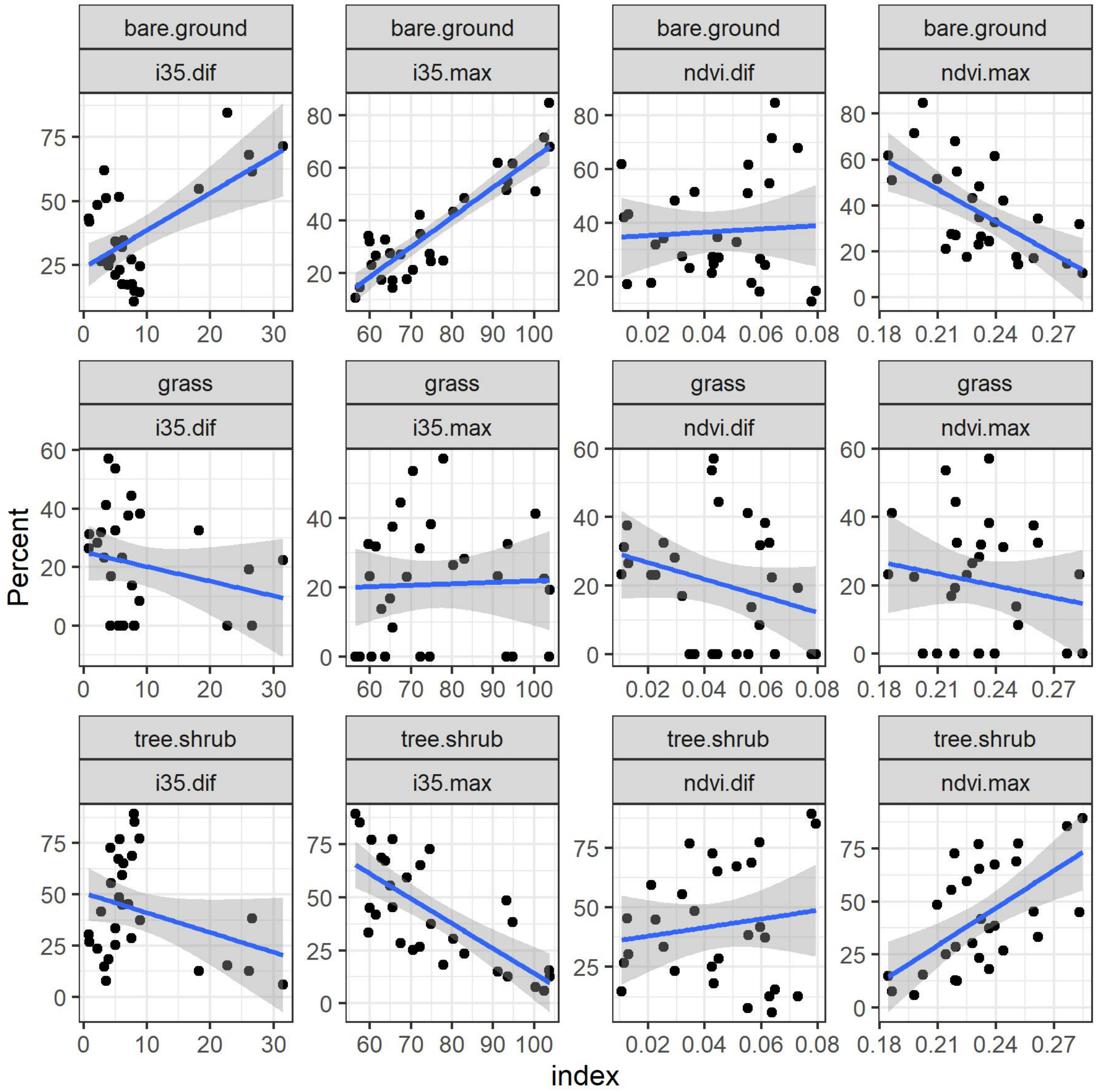

Figure 5: Cover type from the calibration tiles against a range of indices from Landsat data. The "max" plots use the maximum index value from 2019, whereas the "dif" plots use the difference between the maximum and minimum index values from 2019.

Table 3:Correlation coefficients for indices and cover classes.

class	index	Classification with LiDAR and RGB imagery Correlation (r^2)	Classification with RGB imagery Correlation (r2)
Bare ground	i35.max	**0.895**	0.879
Tree/shrub	i35.max	0.724	0.71

Bare ground	ndvi.max	0.615	0.613
Bare ground	i35.dif	0.611	0.58
Tree/shrub	ndvi.max	0.597	0.553
Tree/shrub	i35.dif	0.312	0.307
grass	ndvi.dif	0.293	0.323
grass	i35.dif	0.242	0.222
Tree/shrub	ndvi.dif	0.155	0.189
grass	ndvi.max	0.153	0.103
Bare ground	ndvi.dif	0.069	0.037
grass	i35.max	0.02	0.026

As the “bare ground” class is the inverse of a combined vegetation cover class (grass + tree/shrub classes), correlations between vegetation cover percent, classified using LiDAR and RGB variables) and a range of indices was then tested (Figure 6). The i35 (0.918) and SATVI (0.923) indices recorded the highest correlations.

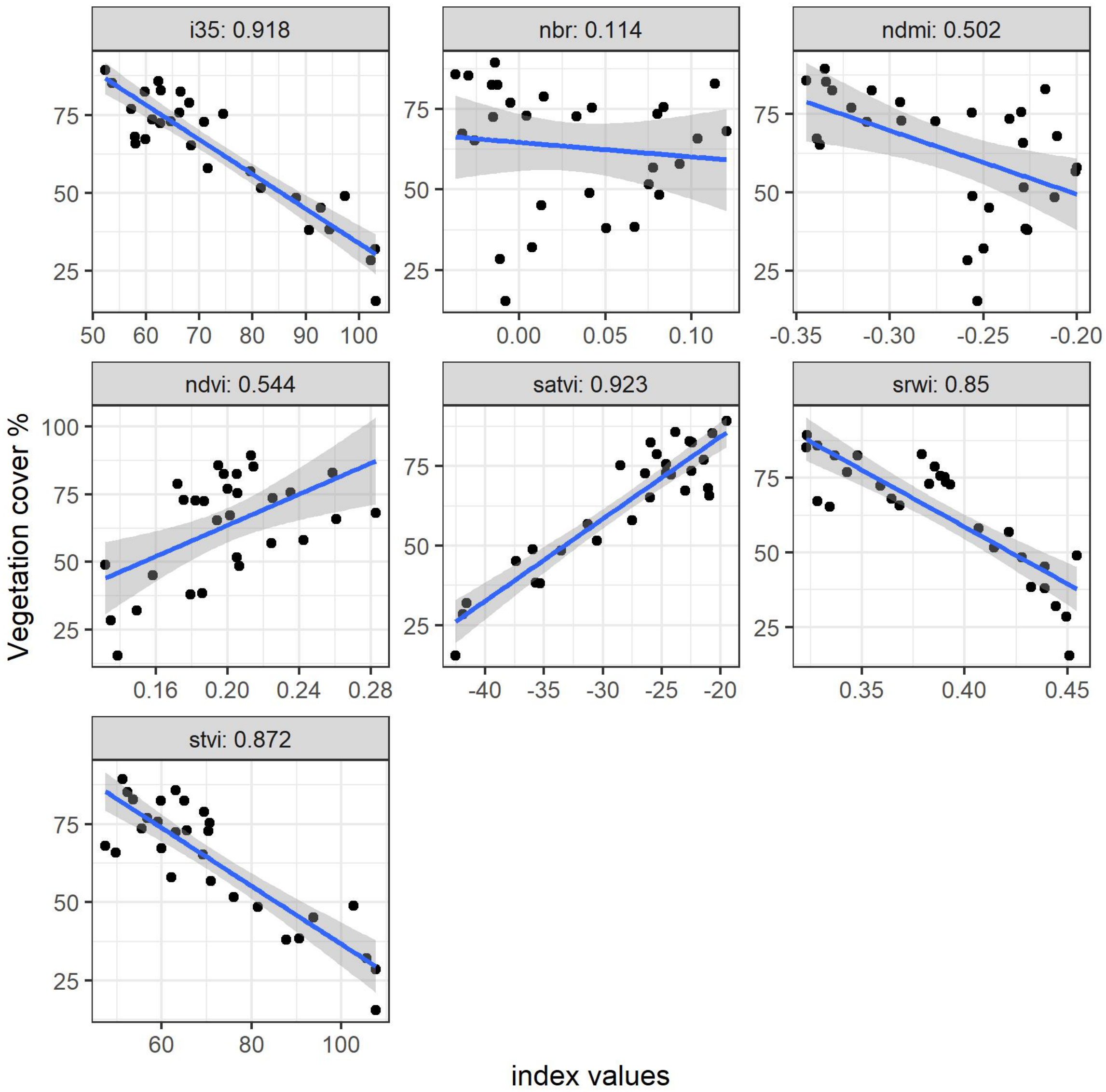

Figure 6: Regression of vegetation cover (classified using LiDAR and RGB variables) against a range of indices from Landsat imagery.

Parameters from the regression with the i35 index (Equation 1) can then be applied to all Landsat imagery to create vegetation cover maps (Figure 7), through the following equation:

Equation 1: Vegetation cover percent from i35.

$$Vegetation\ Cover\ \% = (i35\ \times\ -1.106) + 144.5$$

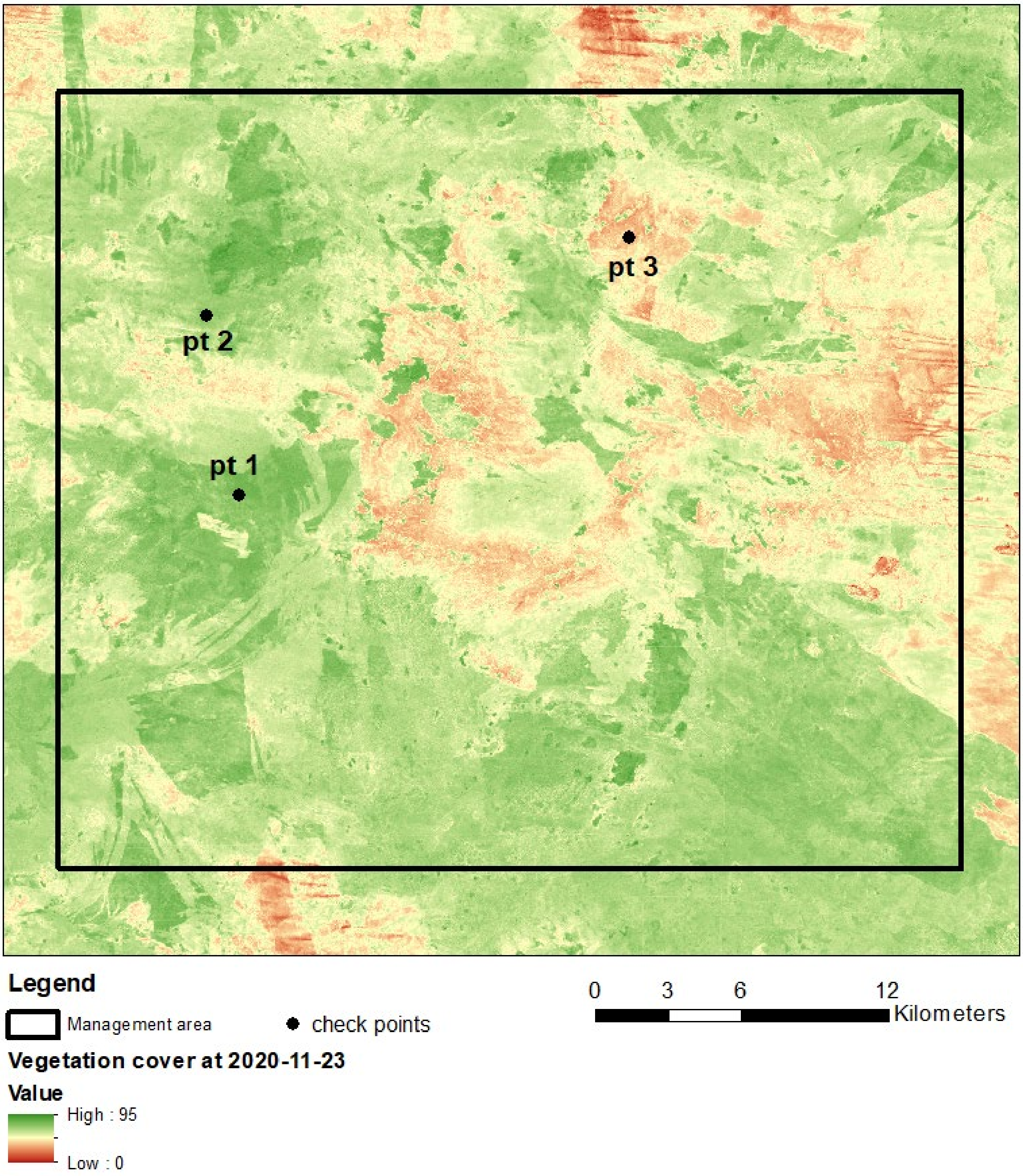

Figure 7: Vegetation cover map from a Landsat image, captured on 23/11/2020, of the management area in the Great Victoria Desert.

The values in the vegetation cover map are somewhat related to the patterns in a "years since last burn" (YSLB) map (Figure 8). Areas of recent fire (low YSLB values) will generally also have low cover values.

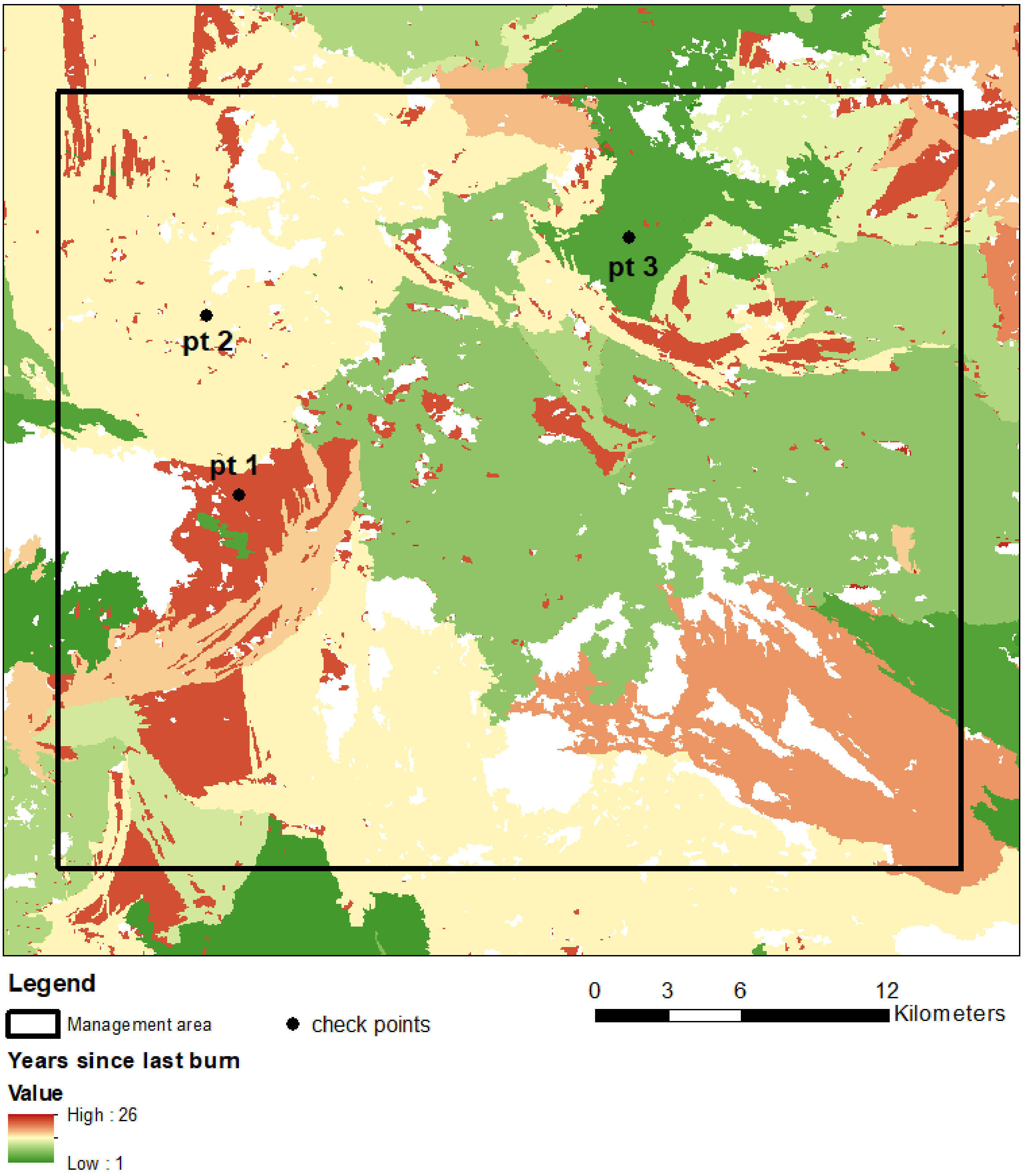

Figure 8: A years since last burn map of the management area in the Great Victoria Desert. Fire maps from 1995 to 2020 were used to create the map.

The complementary information contained in the years since last burn and current vegetation cover datasets can be combined to produce a "fire recovery" dataset. The fire recovery dataset shows percent to which the current cover level is above or below the cover value at which an area previously burnt. For example, check point 1 is in an area with values above 100, this indicates that the current cover level is above the level at which it previously burnt. This difference is highlighted in a time series graph of this point (Figure 10). The graph shows that over the 1988 to 2021 period the point increased in cover from 1988 to around 1998, at this time it burnt, following the burn cover increased rapidly before plateauing for a few years around 2010, after which it increased again. The current vegetation cover level is well above the level when it previously burnt. This represents a predicted high fire risk.

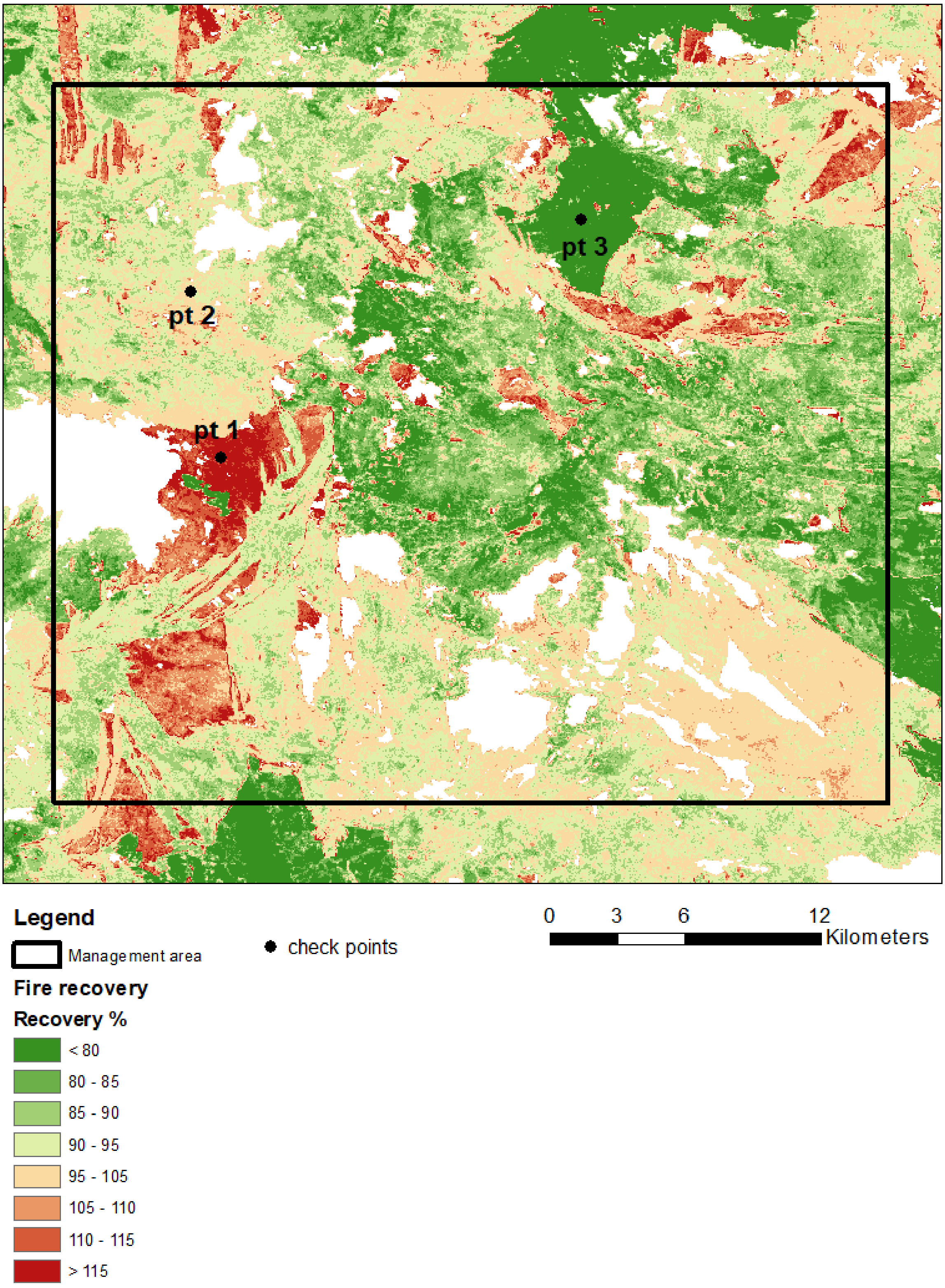

Figure 9: A predicted fire recovery dataset across the management area within the Great Victoria Desert.

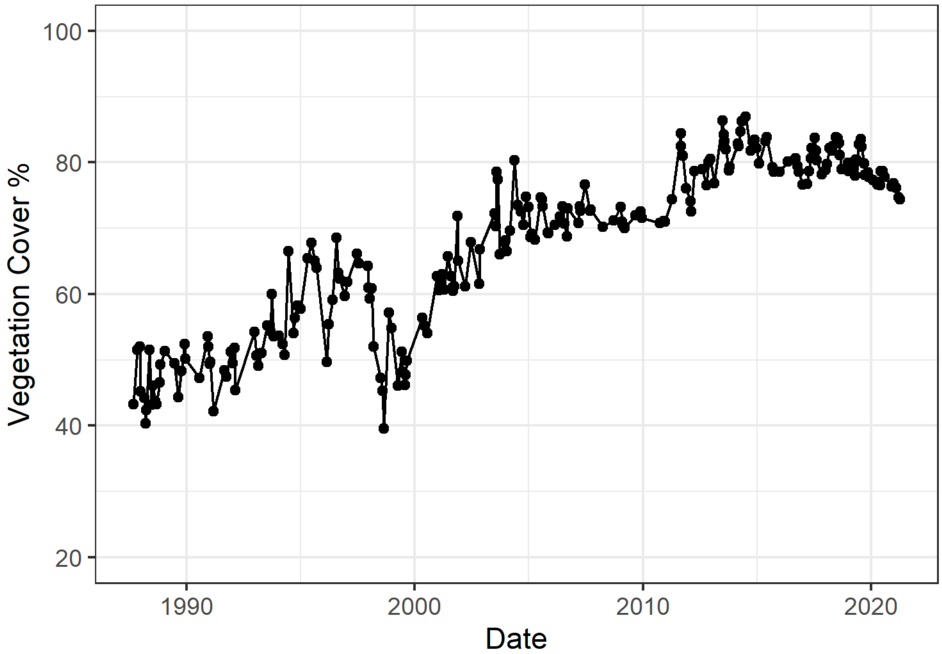

Figure 10: A time series graph of vegetation cover at check point 1.

The area around check point 2 is at similar level to when it previously burnt. This is confirmed by the vegetation time series graph (Figure 11).

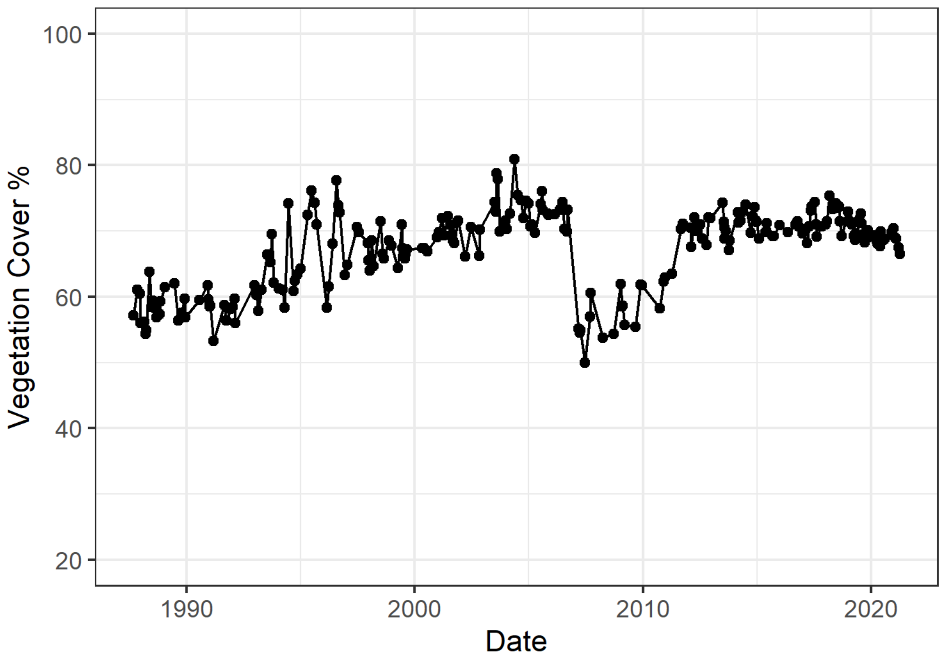

Figure 11: A time series graph of vegetation cover at check point 2.

The area around check point 3 is well below the value when it previously burnt. This can also be seen in the time series graph. The current vegetation cover level ~ 20% is well below the ~80% it was prior to the fire in 2014.

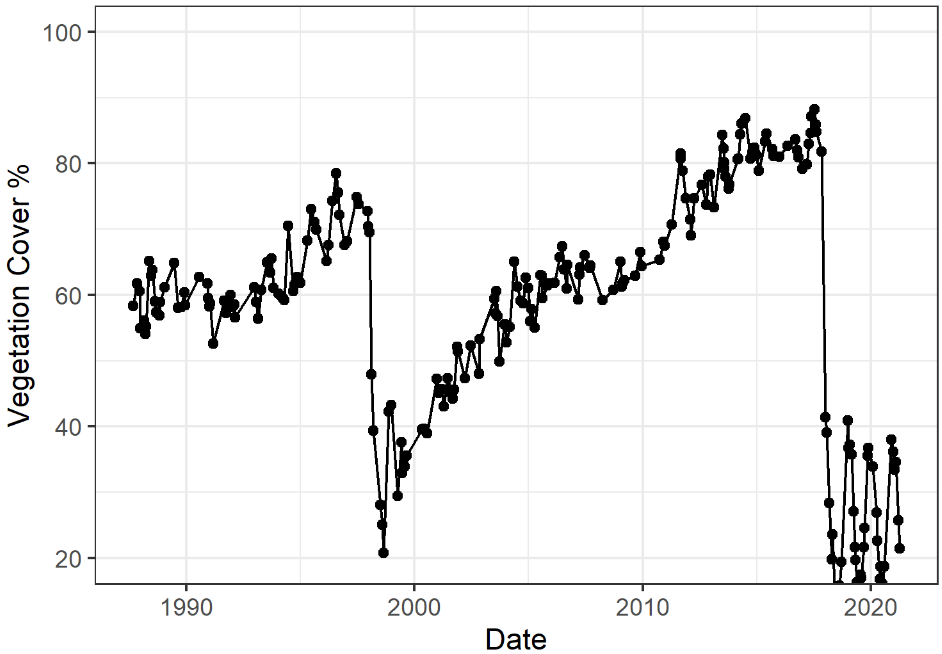

Figure 12: A time series graph of vegetation cover at check point 3.

References

Burrows, Neil, Malcolm Gill, and Jason Sharples. 2018. “Development and Validation of a Model for Predicting Fire Behaviour in Spinifex Grasslands of Arid Australia.” *International Journal of Wildland Fire* 27 (4): 271–79. https://doi.org/10.1071/WF17155.

Lehmann, Eric A., Jeremy F. Wallace, Peter A. Caccetta, Suzanne L. Furby, and Katherine Zdunic. 2013. “Forest Cover Trends from Time Series Landsat Data for the Australian Continent.” *International Journal of Applied Earth Observation and Geoinformation* 21 (April): 453–62. https://doi.org/10.1016/j.jag.2012.06.005.

Marsett, Robert C., Jiaguo Qi, Philip Heilman, Sharon H. Biedenbender, M. Carolyn Watson, Saud Amer, Mark Weltz, David Goodrich, and Roseann Marsett. 2006. “Remote Sensing for Grassland Management in the Arid Southwest.” *Rangeland Ecology & Management* 59 (5): 530–40. https://doi.org/10.2307/3900013.

Qarallah, Bassam, Malik Al-Ajlouni, Ayman Al-Awasi, Mohammad Alkarmy, Emad Al-Qudah, Ahmad Bani Naser, Amani Al-Assaf, et al. 2021. “Evaluating Post-Fire Recovery of Latroon Dry Forest Using Landsat ETM+, Unmanned Aerial Vehicle and Field Survey Data.” *Journal of Arid Environments* 193 (October): 104587. https://doi.org/10.1016/j.jaridenv.2021.104587.

Ruscalleda-Alvarez, Jaume, Dorian Moro, and Richard Van Dongen. submitted. “A Multi-Scale Assessment of Fire Scar Mapping in the Great Victoria Desert of Western Australia.” *International Journal of Wildland Fire*. https://doi.org/10.1071/WF21019.

Schroeder, Wilfrid, Patricia Oliva, Louis Giglio, Brad Quayle, Eckehard Lorenz, and Fabiano Morelli. 2016. “Active Fire Detection Using Landsat-8/OLI Data.” *Remote Sensing of Environment*, Landsat 8 Science Results, 185 (November): 210–20. https://doi.org/10.1016/j.rse.2015.08.032.

Wulder, Michael A., Jeffrey G. Masek, Warren B. Cohen, Thomas R. Loveland, and Curtis E. Woodcock. 2012. “Opening the Archive: How Free Data Has Enabled the Science and Monitoring Promise of Landsat.” *Remote Sensing of Environment*. https://doi.org/10.1016/j.rse.2012.01.010.